Mass Spectrometry—Not Just a Structural Tool: The Use of Guided Ion Beam Tandem Mass Spectrometry to Determine Thermochemistry

P. B. Armentrout
Department of Chemistry, University of Utah, Salt Lake City, Utah, USA

Guided ion beam tandem mass spectrometry has proved to be a robust tool for the measurement of thermodynamic information. Over the past twenty years, we have elucidated a number of factors necessary to make such thermochemistry accurate. Careful attention must be paid to the reduction of the raw data, ion intensities versus laboratory ion energies, to a more useful form, reaction cross sections versus relative kinetic energy. Analysis of the kinetic energy dependence of cross sections for endothermic reactions can then reveal thermodynamic data for both bimolecular and collision-induced dissociation (CID) processes. Such analyses need to include consideration of the explicit kinetic and internal energy distributions of the reactants, the effects of multiple collisions, the identity of the collision partner in CID processes, the kinetics of the reaction being studied, and competition between parallel reactions. This work provides examples illustrating the need to consider this multitude of effects along with details of the procedures developed in our group for handling each of them. (J Am Soc Mass Spectrom 2002, 13, 419–434) © 2002 American Society for Mass Spectrometry

When does a mass spectrometer become an ion beam instrument? Is this defined by the instrument, by whether the operator is an analytical or physical chemist, or by the experiments done? All mass spectrometers utilize ion beams, but the unspoken definition of an ion beam instrument is an apparatus that can be used to make quantitative physical measurements. In this regard, the capabilities of the instrumentation and the intent and training of the operator are all important factors. Whereas a mass spectrometer is often used as an identification tool through the use of mass spectral patterns, by taking advantage of the ability to easily change the kinetic energy of ions, it can also be a powerful instrument for the determination of thermodynamic data.

In this article, I lay down some of the founding principles behind our use of tandem mass spectrometry, and in particular, so-called guided ion beam mass spectrometry to elucidate thermochemical information. This is achieved primarily by examining the kinetic energy dependence of endothermic ion-molecule reactions and determining their energy thresholds. Although many types of instruments have been used to perform such measurements, the link between such studies and guided ion beam techniques is a strong one. Indeed, the NIST Webbook [1] states in its section on Determinations of Reaction Endothermicity that "more commonly a so-called guided-beam apparatus is utilized for such determinations." Considering that there are only about a dozen such laboratories worldwide, this is a testament to the ability of this particular kind of apparatus to provide a plethora of high quality information. However, such information requires attention to myriad details, which are outlined in this article.

Two fundamental types of reactions can be used to acquire thermodynamic information: Bimolecular exchange reactions, process 1, and collision-induced dissociation (CID), process 2.

$$M^+ + AB \rightarrow MA^+ + B \quad (1)$$

$$MA^+ + Rg \rightarrow M^+ + A + Rg \quad (2)$$

Reactions 1 can be either exothermic or endothermic. The threshold for an endothermic bimolecular exchange reaction is given by the difference between the bond energy for the AB reactant, D(AB), and the MA^+ product, $D(MA^+)$. As D(AB) is generally known, mea-

Published online March 26, 2002

Address reprint requests to Dr. P. B. Armentrout, Department of Chemistry, University of Utah, 315 South 1400 East Rm. 2020, Salt Lake City, UT 84112. E-mail: armentrout@chemistry.utah.edu

1044-0305/02/$20.00
PII S1044-0305(02)00347-1

Received November 13, 2001
Revised December 8, 2001
Accepted December 8, 2001

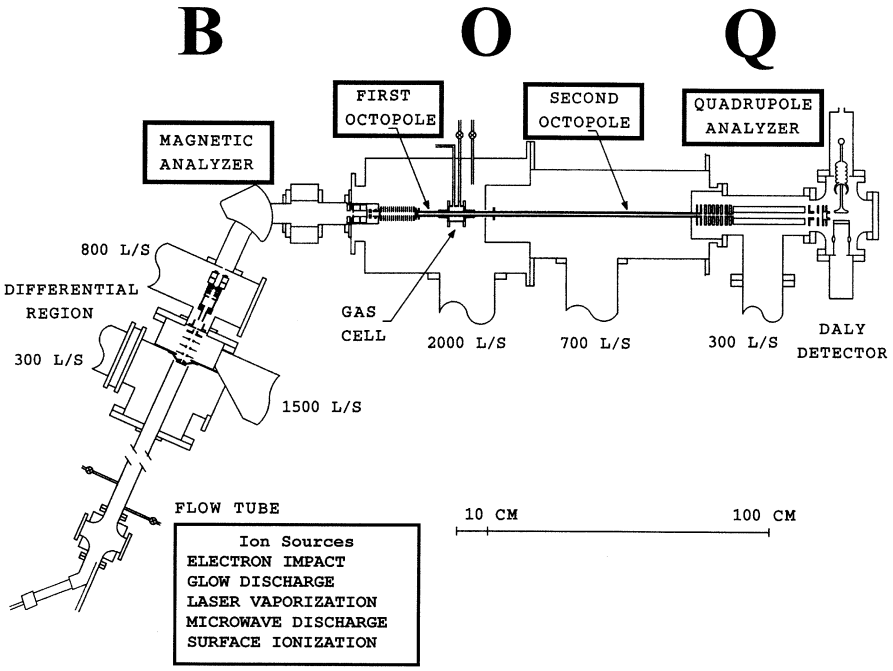

Figure 1. Schematic diagram of one of our guided ion beam tandem mass spectrometers. The main sections of the apparatus are indicated along with pumping capabilities and ion source possibilities.

surement of the threshold, E_0, provides $D(MA^+)$ straightforwardly. CID processes 2 are intrinsically endothermic as a stable bond is being broken. Hence the CID threshold is simply equal to $D(MA^+)$. For both types of systems, the equivalence of thresholds with such thermodynamic properties relies on the assumption that there are no activation barriers in excess of the endothermicity of the reactions. In many respects, this is a key reason to perform such studies with ions because the intrinsic long-range ion induced dipole potentials involved help overcome the types of small barriers commonly observed for neutral systems [2, 3]. Certainly, this assumption need not apply in all systems studied; for instance, restrictions resulting from spin or orbital angular momentum conservation can occur [3, 4]. Such issues must be assessed for each system of interest. For CID processes, the quantum mechanical properties of the electronic potential energy surfaces have been evaluated [5], and confirms that this assumption is applicable for heterolytic bond cleavages, whereas systems that dissociate homolytically need individual assessment.

The range of systems amenable to guided ion beam studies is extremely broad. For example, we have used reactions 1 to measure the binding energies of ionic transition metal atoms and clusters to ligands such as H, OH_x (x = 0–1), NH_x (x = 0–2), C_yH_x (y = 1–4, x = 0–2y + 1), SH_x (x = 0–1), and SiH_x (x = 0–3). CID studies have encompassed an even broader range of systems including metals throughout the periodic table and ligands such as rare gas atoms, H_2, N_2, CO, NO, CO_2, H_2O, NH_3, CH_4, larger alkanes, C_2H_4, larger alkenes, alkynes, alcohols, amines, ethers, aldehydes, ketones, crown ethers, benzene, substituted benzenes, azoles, azines, amino acids, and nucleic acids. In our laboratory, studies have included over 50 different elemental ions. Continued work in our group and others is only expanding this list.

The Guided Ion Beam Tandem Mass Spectrometer (BOQ)

Our guided ion beam tandem mass spectrometers (GIBMS) have been specifically designed and constructed to allow precise control over the kinetic energy of reactant ions in the region where they interact with neutral reagents. In this regard, they differ from most commercial instruments in that the interaction region is physically larger than the mass spectrometers. Further, the design principles centered around the idea that *transmission of the ions is more important than mass resolution*. Otherwise, accurate absolute reaction cross sections cannot be measured. One of our GIBMS instruments is shown in Figure 1 [6, 7]. Both of our instruments have three sections in a BOQ (magnetic sector, octopole, quadrupole) arrangement sandwiched between the ion source and detector. The second apparatus differs from that shown primarily in the source region and because it has no second octopole [8].

A magnetic sector was chosen for the initial mass analysis device to provide unit mass resolution, good transmission, and a well-focused ion beam. As most experiments generally employ only a single reactant ion, this magnetic sector does not need to be actively scanned during experiments. Focusing lenses before

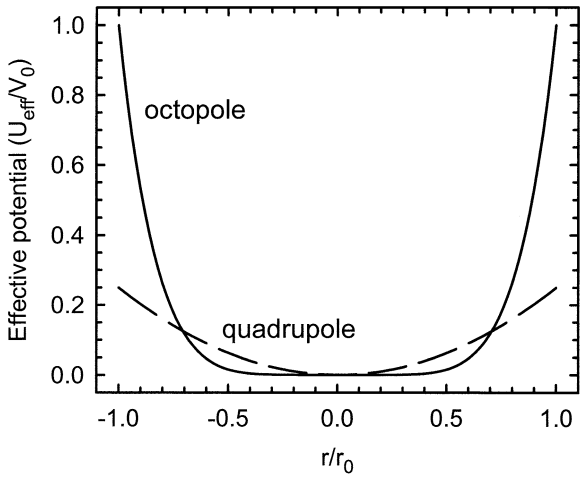

Figure 2. The reduced effective potential of an octopole and quadrupole radiofrequency trap as a function of the fractional distance between the center of the device and the rods.

and after the sector enhance ion transmission. An exponential retarder lens system is used to decelerate the ions to low energies while retaining a good focus and low energy dispersion [9]. This provides an ion beam with well-defined energies along the axis of the instrument and low radial velocities (in contrast to the use of an initial quadrupole mass analyzer).

The octopole ion beam guide is a rf-only device pioneered by Teloy and Gerlich [10, 11]. Details of such inhomogeneous radiofrequency devices are provided in a comprehensive review by Gerlich [12]. The advantages of a rf trapping field in the interaction region include enhanced collection efficiency of scattered reactant and product ions and the ability to extend the usable energy region below about 1 eV (lab) down to thermal energies, about 0.04 eV (lab). The key advantage of an octopole over the conceptually similar rf-only quadrupole is that a more homogeneous trapping field is obtained with more rods. In addition, the time-averaged radial trapping field of a rf multipole device can be shown to vary as r^{p-2}, where r is the distance away from the center of the device and p is the number of poles [6, 12]. Thus, a quadrupole has an effective trapping field that is quadratic, $p - 2 = 2$, whereas the octopole field varies as r^6. These fields are shown in Figure 2. Because the octopole field has a relatively flat region in its center, it perturbs the ion energy in the radial direction much less than the quadrupole field, providing much better defined ion energies. In addition, the depth of the trapping field varies as $(p/2)^2$ such that the octopole field provides a four-fold stronger potential than the quadrupole for the same applied voltage, as shown in Figure 2. In the apparatus shown in Figure 1, a second octopole has recently been added [7]. This device is designed for chemical physics experiments in which the velocities of the ions are measured in both the axial and radial directions, such that full three-dimensional maps of the product ions can be ascertained [7, 12–14]. For the experiments discussed in the present work, the presence of this second octopole is largely benign, being neither beneficial nor a hindrance.

We chose a quadrupole mass filter for the second mass analyzer because this device provides good throughput for ions having widely varying trajectories (as product ions tend to display). In general, the quadrupole is operated at the lowest resolution necessary to resolve reactant and product ions in order to keep transmission high. A key component of this instrument is the lens system between the octopole and quadrupole. These lenses need to efficiently transport ions emerging from the octopole (which can have large radial velocities because of the rf voltages) into the quadrupole. Finally, the detector chosen was a Daly detector [15], which incorporates a high voltage first dynode held at about 25 kV or higher. This detector provides near unit sensitivity for counting ions.

Ion Sources

Another feature of our GIBMS instruments is the versatility of the ion sources. In early work, we utilized electron impact and surface ionization sources as a means to alter and control the extent of internal energy in the reactant ions produced. Later, we developed a flow tube source that provides extensive collisional cooling of the ions (about 10^5 collisions) and allows chemical reactions (notably, three-body condensation) as well [16]. For ion production, the flow tube can be connected to microwave discharge, dc (glow) discharge, electron impact, or laser vaporization ion sources. To study reactions of metal cluster cations, we also developed a laser vaporization/supersonic expansion source, in essence a mini-flow tube [17]. This source is still unique in that it uses a copper vapor laser operating at 7 kHz, thereby making a quasi-continuous metal cluster ion beam. Presently, we are also developing an electrospray ion source to couple to the flow tube. This variety of sources provides great flexibility in generating ions under well-controlled conditions, as illustrated in the results described below.

Conversion of Raw Data

In a typical GIBMS experiment, reactant ions are selected using the initial momentum analyzer and focused into the collision cell containing the reactant neutral of choice. A mass spectrum of the resulting ions is taken using the quadrupole mass filter to determine what products are formed. Generally, this is performed at several ion kinetic energies, which are determined by varying the dc voltage applied to the octopole. Ion intensities of the reactant and product ions are then measured while sweeping the ion kinetic energy, including through the region where the reactant ions no longer have enough energy to pass through the octopole. On alternate energy sweeps, the neutral gas is directed into the vacuum chamber, but not into the collision cell. The resultant raw data are reactant and

product ion intensities (both with and without gas in the cell) as a function of the ion kinetic energy. To convert these data to a more usable form that is independent of the instrument used to acquire the data, several transformations are required. One involves converting from the kinetic energy of the ion, the laboratory energy, to the center-of-mass energy, the energy available to the reaction system for chemical transformations. A second involves converting the ion intensities to cross sections, which represent the intrinsic probability for reaction.

Absolute Zero of Energy

If the energy scale for reaction is to be known accurately, then it is clearly important that the zero of this scale be ascertained. Indeed, we have documented examples in the literature where an understanding of the reaction was hindered for years by the failure to independently assess where the absolute zero of energy was located [18]. Experimentally, this can be difficult because the potentials where the ions are formed and where they react may not equal the applied potentials. Differences of several volts can be realized as a consequence of contact potentials, field effects (especially in the ion source), space charge effects, and surface charging. In our instruments, the zero of the ion energy is routinely determined for each experiment by measuring the reactant ion intensity as a function of the dc bias potential applied to the entire octopole as this is swept through the zero of energy. This sweep gradually cuts off ions with less energy than the applied voltage. Because the retarding measurement and reactions are performed in the same physical region of the apparatus, ambiguities with regard to contact potentials and field, space charge, and surface charging effects in the ion source are eliminated. These latter effects are less likely in the reaction region because of the much lower ion intensities here. In early ion beam experiments, retardation methods were notoriously difficult because the slow moving ions were very easily lost. However, such problems are avoided here because of the trapping characteristics of the octopole ion beam guide. The resulting retardation curve is differentiated to yield a direct measurement of the distribution of ion kinetic energies. Ordinarily, this curve is nearly Gaussian in shape. By fitting a Gaussian function to the entire data set, the center of the peak, which equals the absolute zero of energy, can be determined with a precision of 0.05 eV (lab). The full width at half maximum varies with the ion source, but widths of 0.2 eV (lab) are routinely obtained. Such retardation measurements can be adversely influenced by potential barriers along the octopole (e.g., when it is dirty), such that the energy zero can be shifted to slightly higher energies. However, the accuracy of the energy scale measured using this retardation procedure has been verified by time-of-flight measurements [6, 7], which are more time consuming than the retardation methodology but are based on a potential averaged over the entire length of the octopole. The agreement between the two methods indicates that the retardation measurements are adequate for routine work as long as the cleanliness of the octopole is maintained.

Laboratory to Center-of-Mass Energies

In measuring thermodynamic quantities, it is critical to know how much energy is available to the reaction system. In any collision experiment, the translational energy of the two colliding particles can be broken down into two parts: The relative translational motion of the two reactants and the motion of the entire collision system through the laboratory. Because of conservation of linear momentum, the energy tied up in the latter part is conserved and therefore unavailable for inducing chemical change during the reaction. Hence the relative kinetic energy of the two particles, the so-called center-of-mass energy, E_{CM}, is the quantity of interest in determining threshold phenomena. In beam-gas experiments like those performed using our GIBMS instruments, the neutral reactant is essentially stationary (on average, this is explicitly so) whereas the ion has an appreciable velocity defined by its laboratory energy, E_{lab}. This circumstance leads to a particularly simple expression for converting from E_{lab} to E_{CM}, namely, $E_{CM} = E_{lab}\, m/(m + M)$ where m and M are the masses of the reactant neutral and ion, respectively. This formula accurately describes the mean of the energy distributions, however, the kinetic energies of both the ion and the neutral have distributions that must be explicitly considered in the data analysis, as described further below. In addition, this expression fails if the entire distribution is not present, such as when the ion beam energy distribution is truncated at low energies. Corrections for such truncations are straightforwardly made and are necessary at very low kinetic energies [6].

The necessity for the laboratory to center-of-mass conversion is nicely illustrated in Figure 3. Here, cross sections for reactions 3 and 4 are displayed on both the laboratory and center-of-mass energy scales.

$$W^+ + H_2 \rightarrow WH^+ + H \quad (3)$$

$$W^+ + D_2 \rightarrow WD^+ + D \quad (4)$$

Because the H_2 and D_2 reactants are so much lighter than the W^+ reactant, the $m/(m + M)$ factors are very small, 0.011 and 0.021, respectively, but differ from each other by a factor of approximately 2. Note that the experimental results for H_2 and D_2 differ appreciably when plotted versus E_{lab}, but are nearly superimposable when plotted versus E_{CM}, as expected for chemical processes that differ only by isotopic substitution. Indeed, the small differences that remain are real and result from the zero point energy differences in $D_0(H_2)$

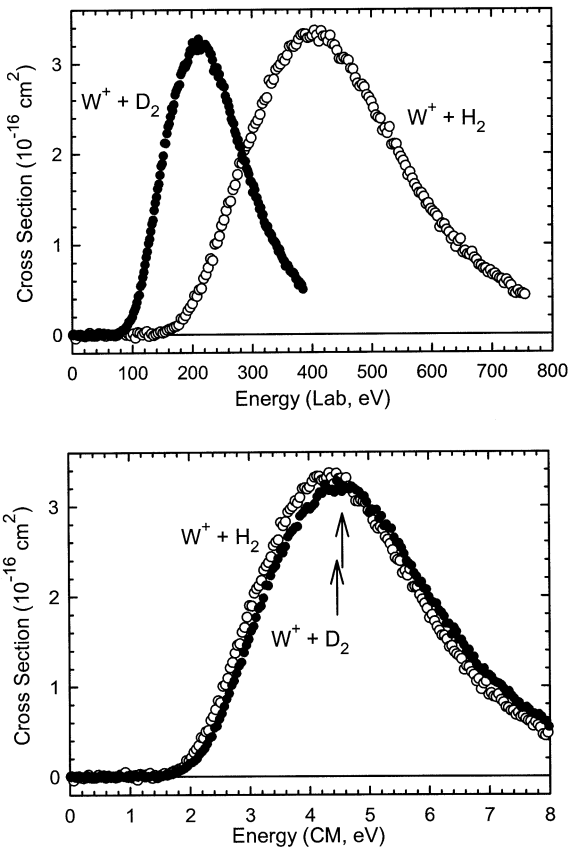

Figure 3. Experimental cross sections for reactions 3 (open circles) and 4 (closed symbols) as a function of laboratory energy, part **a**, and center-of-mass energy, part **b**. Arrows in part **b** indicate the bond energies of the H_2 and D_2 reactants at 4.478 and 4.556 eV, respectively.

= 4.478 eV versus $D_0(D_2)$ = 4.556 eV [19] and $D_0(WH^+)$ versus $D_0(WD^+)$ [20].

A further verification that the center-of-mass scale is the appropriate scale for thinking about chemical observations comes from the position of the peaks of these two cross sections. In both cases, the probability for forming WH^+ (WD^+) reaches a maximum at the energy where the product can begin to dissociate in the overall processes 5. These reactions have onsets equal to $D_0(H_2)$ and $D_0(D_2)$.

$$W^+ + H_2\ (D_2) \rightarrow W^+ + 2\ H\ (D) \qquad (5)$$

Note that the cross sections peak very close to these energies on the center-of-mass scale, but no such correspondence is associated with the laboratory scale energy.

Correction for Background Signals

Because there is a background pressure of the neutral reagent in the instrument, reactions can occur both inside the collision cell and outside. In our instruments, the octopole is at least twice as long as the collision cell, such that the regions immediately outside the gas cell (where the pressure might still be appreciable) are still inside the octopole, Figure 1. Thus, the kinetic energy of the ions does not vary throughout the region where ion-molecule collisions are probable. This feature is a distinct advantage and differs from triple quadrupole (QQQ) instruments where the gas cell extends to the end of the central quadrupole. In most QQQ designs, collisions outside the gas cell occur in the other two quadrupoles, where the ion energies differ because they are chosen for mass resolution and transmission purposes.

Even in our instruments, however, the contributions of reactions outside the confines of the collision cell need to be accounted for because, although the pressures may be low, the path lengths can be long. In our experiments, this is accomplished by measuring the product and reactant ion intensities with the neutral gas no longer directed to the gas cell, but merely allowed into the vacuum chamber. This provides the same background pressure of neutral gas in all regions of the instrument but the collision cell. Hence, product ion intensities resulting from reactions outside the collision cell along with background noise in the detection circuitry are explicitly measured and subtracted from the signals obtained with gas directed to the cell. These corrections are particularly important for threshold measurements, where *it is critically important to know where zero signal is* (so you know when you have a non-zero signal). Approximately half of the time spent in all our experimental measurements is used in determining where zero signal is.

Intensities to Cross Sections

The reaction cross section, σ, is the intrinsic property in collision/reaction theory that describes the probability that two particles, here an ion and a neutral, collide and proceed to products. A cross section has units of area and is profitably thought of as the effective size of the ion-molecule collision pair. Hence, units of 10^{-16} cm^2 or equivalently, Å^2, are generally used. Multiplication of the cross section by the relative velocity of the reactants, v, gives a rate constant, $k(E) = \sigma v$. Averaging over a Maxwell-Boltzmann distribution gives the more familiar $k(T) = <\sigma v>_{MB}$. Thus, a cross section can be thought of as a microscopic reaction probability directly related to the rate constant for reaction at a specific kinetic energy.

Calculation of the cross section from the ion intensities utilizes a relationship that is directly analogous to the Beer-Lambert Law, specifically,

$$I = I_0 \exp(-\rho\sigma\ell) \qquad (6)$$

where I is the reactant ion intensity after passing through the collision cell, I_0 is the reactant ion intensity entering the collision cell, ℓ is the length of the collision cell, and ρ is the number density of the neutral reactant,

$= P/k_BT$ where P and T are the pressure and temperature of the gas and k_B is the Boltzmann constant. Clearly if no ions are lost during the collision and detection process, then $I_0 - I = \Sigma I_p$, the sum of the intensities of all product ions. As noted above, one of the key advantages of the guided ion beam method is to enhance the collection efficiency of product and scattered reactant ions, such that this relationship is effectively realized. In the thin-target limit, which can occur for either small ℓ or ρ, the exponential term in eq 6 reduces to $(1 - \rho\sigma\ell)$ and we can write that $\Sigma I_p = I_0 - I = I_0\rho\sigma\ell$ or that $\sigma = \Sigma I_p/(I_0\rho\ell)$. We ordinarily use the exponential form to reduce our data. Reaction cross sections for individual product ions are given by $\sigma_p = \sigma\,(I_p/\Sigma I_p)$.

To experimentally evaluate the cross section, each of the terms in eq 6 must be determined. Certainly the measurement of ion intensities is straightforwardly done in mass spectrometry, although efficient collection and detection is clearly important if the final absolute cross section is to be accurate. Measurements of the pressure (good to about 10%) and temperature (very accurate) of the neutral reactant, as needed for ρ, are also straightforwardly made. Technically, there is really a pressure profile for any collision cell because of the open apertures necessary to let the ions in and out, Figure 1. The effects of this profile are generally incorporated into the quantity ℓ, which could simply be the physical length of the collision cell, but is generally defined as an effective length, meaning that it accounts for the distribution in pressures across its length. In our instruments [6–8], we designed our collision cells to have central regions of well-defined length and pressure with tubes that tightly surround the octopole, Figure 1. The pressure is presumed to decrease linearly in these tubes to the background pressure, which is about 100 times smaller than the cell pressure given the pumping in our instruments. This gives a trapezoidal pressure profile such that the effective length of the collision cell is equal to the length of the central portion plus one/half the length of the two tubes. The accuracy of this characterization, presumed to have an uncertainty of about 10%, is evaluated as described next.

Assessment of the Accuracy of the Absolute Cross Sections

When we assembled our first GIBMS, we sought to test whether the assumptions regarding the gas cell length and collection efficiency were valid. In doing this, we examined several test systems where absolute cross sections had been measured previously by others. Our original idea was to use these previous results to empirically determine our effective gas cell length, but such comparisons have consistently shown that no empirical correction is needed. Our instruments provide absolute cross sections that are the equal of any measured elsewhere.

One of these systems, $Ar^+ + H_2 \rightarrow ArH^+ + H$, was published and clearly demonstrated the abilities of the GIBMS to measure accurate absolute cross sections as a function of energy [6]. We found excellent agreement between our data and that from previous beam studies that measured cross sections at higher energies and drift tube studies that determined rate constants as a function of energy at lower energies. Subsequently, we also tested our methods directly against theory, showing for instance that the exothermic $O^+(^4S) + H_2\,(D_2) \rightarrow OH^+\,(OD^+) + H\,(D)$ reactions have cross sections within a few percent of theoretically predicted cross sections at low energies [21]. Another example is shown in Figure 4, which shows early, unpublished work on the exothermic reaction $N_2^+ + H_2 \rightarrow N_2H^+ + H$, confirmed some eight years later by subsequent studies [22]. The figure shows that our cross sections agree very well with two previous studies [23, 24], which span a typical energy range for ion beam experiments without ion guides. At low energy, our cross sections also agree nicely with several room temperature rate constant measurements (see [22] for references) approximately converted to cross sections and with the theoretical collision cross section [25]. The deviations between experiment and the predicted collision cross section at intermediate energies (>0.02 eV) are real and discussed in detail in our subsequent work [22]. In this work, our cross sections at low energies were converted to a thermal rate constant of $1.7 \pm 0.4 \times 10^{-9}$ cm^3/s. This can be compared with eleven literature values, which range from 1.4–2.2 $\times 10^{-9}$ cm^3/s and average to $1.7 \pm 0.3 \times 10^{-9}$ cm^3/s, and with the collision rate of 1.56×10^{-9} cm^3/s [25].

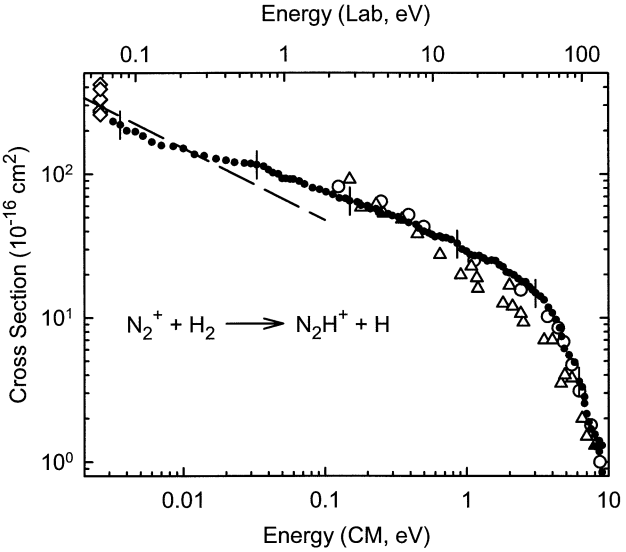

Figure 4. Experimental cross sections for the reaction of N_2^+ with H_2 (closed symbols) as a function of laboratory energy, upper x-axis, and center-of-mass energy, lower x-axis. Open circles and triangles show results taken from Turner et al. [23] and Hierl et al. [24], respectively. At low energy, open diamonds indicate several room temperature rate constants approximately converted to cross sections. The dashed line indicates the theoretical collision cross section [25]. Vertical bars on a few data points indicate 20 % uncertainties in the guided ion beam results.

Important Factors in the Data Analysis

Over the course of the last two decades, our research into the kinetic energy dependence of ion-molecule reactions has evolved considerably. We have elucidated a number of factors that must be considered in order to extract accurate thermodynamic information from such studies. These various factors are described and illustrated in the following sections.

A Simple Model for the Kinetic Energy Dependence of Reactions

There is no simple theory that describes the kinetic energy dependence of chemical reactions. The closest most chemists come to such an expression is the Arrhenius equation, $k(T) = A \exp(-E_a/k_BT)$, which is really just a simple empirical means of parameterizing the temperature dependence of rate constants over finite temperature ranges. To elucidate the kinetic energy dependence of reactions, we similarly turn to a simple empirical formula:

$$\sigma(E) = \sigma_0 (E - E_0)^n / E^m \quad (7)$$

where E is the energy available to the reaction system (E_{CM}), E_0 is the threshold for reaction, σ_0 is an energy independent scaling factor that controls the magnitude of the cross section, and n and m are parameters that control the shape of the energy dependence. At energies below E_0, the model predicts that $\sigma(E) = 0$. The history of this model form has recently been reviewed [26], but can be traced to a variety of different functions (having different values of n and m) that all were developed to describe the kinetic energy dependence of chemical reactions. In addition, it can be noted that multiplying eq 7 by the velocity and averaging over a Maxwell-Boltzmann distribution does yield an Arrhenius-like function for $k(T)$, although A exhibits a temperature dependence that is specified by the particular n and m values.

Over the course of time, we have determined that the use of eq 7 with $m = 1$ generally provides an adequate treatment of the kinetic energy dependence of ion-molecule reactions and one that can be theoretically justified [27]. However, we [28, 29] and others [30] have documented exceptions to this conclusion associated with reactions that are limited by coupling between reaction surfaces of different spin. In such cases, an additional $E^{-1/2}$ factor needs to be introduced such that m is effectively 1.5. As discussed in detail in our most recent work [29], this expression can be justified by appealing to a Landau-Zener model [31, 32] and agrees with several modern theoretical treatments [33, 34] for the kinetic energy dependence of the crossing probability between diabatic surfaces of different spin multiplicities.

The parameter n is an empirical representation of various factors that change the reaction probability and generally varies with the complexity of the system being studied. As discussed elsewhere, values of n can be related to the phase space available to the reaction [26]. For the case of CID reactions, we have recently performed experiments that demonstrate a relationship between the n parameter and the efficiency of energy transfer in the initial collision [7]. This work bolsters the use of eq 7, and its derivatives below, in modeling the kinetic energy dependence of CID reactions.

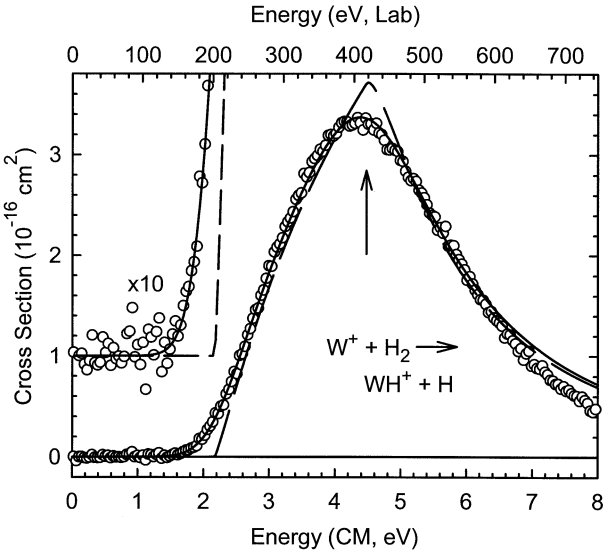

Figure 5. Experimental cross sections for reaction 3 (circles) as a function of laboratory energy, upper x-axis, and center-of-mass energy, lower x-axis. The dashed line shows the model of eq 7 with the parameters given in the text, and a variation of this model at high energies that accounts for reaction 5. The full line shows this model convoluted with the kinetic energy distributions of the reactants. The arrow indicates the bond energy of the H_2 reactant at 4.478 eV.

Translational Motion of the Reactants: Doppler Broadening

In interpreting the thresholds of reaction cross sections using the model function, eq 7, the kinetic energy distributions of the reactants must be included. This was first recognized by Chantry [35], who outlined the mathematical treatment required for the kinetic energy distribution of the neutral species. Lifshitz et al. later extended this to include the kinetic energy distribution of the ionic reactant [36]. The importance of this effect can be seen by examining Figure 5, which shows cross sections for reaction 3 [20]. It can be seen that the apparent threshold, the energy at which the experimental cross section first deviates from zero is about 1.5 eV and then the cross section gradually rises. Combined with $D_0(H_2) = 4.48$ eV, such a threshold energy would mean that $D(W^+–H) \approx 3.0$ eV. This disagrees grossly with a theoretical prediction of 2.16 eV [37].

Figure 5 also shows our model function, eq 7, as the dashed line. When convoluted with the motion of the neutral, so-called Doppler broadening, we obtain the

full line. The kinetic energy distribution of the ionic reactant is negligible here because of the large lab to center-of-mass energy conversion factor. Clearly, the convoluted model reproduces the data with excellent fidelity throughout the low energy range and into the noise level. This good agreement is obtained when the parameters of eq 7 are $\sigma_0 = 6.7$, $n = 1.1$, and $E_0 = 2.18$ eV. This threshold yields $D(W^+–H) \approx 2.3$ eV, in reasonable agreement with the theoretical value. (Our more refined experimental value, $D_0(W^+–H) = 2.27 \pm 0.05$ eV [20], requires careful consideration of the internal energy effects, as discussed below). The Doppler broadening is particularly severe in this case because the neutral reactant is light such that it has a large velocity distribution at room temperature. The accuracy of this treatment has been verified many times and the need to account for the kinetic energy distributions is unambiguous.

The need for including Doppler broadening in the analysis is also illustrated at high energies in Figure 5. As noted above, the dissociation process 5 can begin at $D_0(H_2) = 4.478$ eV. To account for this new process, we incorporate another empirical representation of the kinetic energy dependence of this secondary process, as described in detail elsewhere [38]. In the analysis shown in Figure 5, the model holds the threshold for the dissociation process 5 at its thermodynamic value, adjusting only a parameter that describes the rapidity of the decline. Despite this restriction, the model cross section reproduces the high-energy behavior with very good accuracy. The effects of the thermal motion of the neutral reagent are again evident as the difference between the convoluted and unconvoluted models, Figure 5.

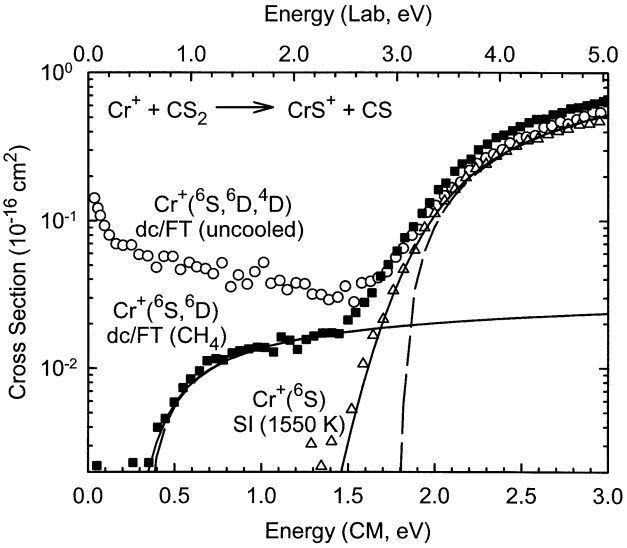

Figure 6. Experimental cross sections for the reaction of chromium cations with carbon disulfide (symbols) as a function of laboratory energy, upper x-axis, and center-of-mass energy, lower x-axis. Results are shown for chromium cations produced in three different ion sources: Surface ionization at 1550 K (open triangles), dc discharge/flow tube (dc/FT) source with methane gas added (closed squares), and the dc/FT source with no cooling gas added (open circles). The dashed lines show the model of eq 7 and full lines show these models convoluted with the kinetic energy distributions of the reactants.

Internal Energy of the Reactants: Electronic

In seeking to understand threshold phenomena, it is important to know about all the energy available to the reactants. In our early work on the reactions of transition metal ions, it became clear that different electronic states of the metal ions could have a strong influence on the observed reactivity [39–43]. This became particularly evident when the reactivity was examined as a function of kinetic energy, as thresholds for reaction would shift depending on the presence or absence of different electronic states. Because the energies of such states can be large (although for transition metal ions, they can also be deceptively small), such shifts can be obvious. An example taken from recent work on the reaction of $Cr^+ + CS_2$ [44] is shown in Figure 6. Three experimental results, which differ in the source used to produce the metal ion, are shown. The coldest source, surface ionization (SI), provides a beam that is 100 % ground state $Cr^+(^6S)$. Analysis of this cross section using eq 7 yields a threshold of 1.79 ± 0.12 eV and thus a Cr^+–S bond energy of 2.71 ± 0.13 eV. When the ions are formed by a dc discharge/flow tube combination (dc/FT), the cross section shows the same cross section at high energies (>1.5 eV) along with a new feature at low energies that exhibits no threshold, i.e., an exothermic reaction similar to the behavior observed in Figure 4. These results indicate that most of the Cr^+ ions formed in the dc/FT source are in the ^6S ground state, but electronic states of Cr^+ having energies in excess of 1.79 eV are present. Such states include the second excited state, ^4D, and above [45]. Methane has been shown to react efficiently at thermal energies with these higher lying states [39, 46–49]. Consequently, when small amounts of methane gas are present in the flow tube source, the excited states are removed leaving behind ions that yield the third cross section shown. This shows an endothermic feature at energies below the threshold for the $Cr^+(^6S)$ cross section. Modeling these low energy data gives a threshold that is 1.36 ± 0.16 eV below that for reaction of $Cr^+(^6S)$. This energy corresponds nicely to the average excitation energy of the ^6D first excited state, 1.522 eV [45]. This state is known not to react with methane at thermal energies [49]. Clearly, electronic energy, E_{el}, is available to the reactants and can drastically alter the appearance of the cross sections and the thresholds observed. Therefore, we alter eq 7 to include this source of energy yielding eq 8.

$$\sigma(E) = \sigma_0 (E + E_{el} - E_0)^n / E \quad (8)$$

If more than one electronic state is involved in the observed reaction, then the expression needs to include

a sum over all states and the fractions of each state in the reactant ion beam.

Internal Energy of the Reactants: Vibrational

Compared with electronic excitation, the influence of vibrational energy on reaction thresholds is more difficult to ascertain unambiguously for two reasons. First, the energies involved can be much less than electronic excitation. Second, except for rare state-specific experiments [50], vibrational excitation is generally available as a distribution characteristic of the temperature of the reactants, meaning that sharp features, such as those observed in Figure 6, are not observed. Because of this distribution of vibrational energies, the shape of the model function, eq 7, is altered by introducing more curvature. Thus, the determination of accurate thresholds cannot be performed by simply adjusting the threshold measured for the average vibrational energy, which we have shown explicitly [3, 51]. To obtain the most accurate thermochemistry from threshold analyses, the entire vibrational energy distribution must be included as an explicit sum over all vibrational states, as shown in eq 9,

$$\sigma(E) = \sigma_0 \Sigma g_{\text{vib}} (E + E_{\text{vib}} - E_0)^n / E \quad (9)$$

where g_{vib} is the population and E_{vib} is the energy of each vibrational state.

One means to determine whether vibrational energy must be included in threshold modeling is to examine systems in which the thermochemistry is already known. An example of such a system is lithium ion water clusters, $Li^+(H_2O)_x$, which have been studied by both CID [52] and high pressure mass spectrometry (HPMS) [53]. Our CID results for the $x = 2$ and 5 clusters are shown in Figure 7. The model of eq 9 is shown convoluted over the kinetic energy distributions of the reactants. Unconvoluted models, i.e., for reactants having internal energies of 0 K and monoenergetic interaction energies, are also shown. It can be seen that the apparent thresholds for these systems are about 1 and 0 eV, respectively. Equilibrium measurements of the $(H_2O)Li^+–OH_2$ and $(H_2O)_4Li^+–OH_2$ bond energies obtained by Dzidic and Kebarle [53] using HPMS provide 298 K bond energies of 108 ± 4 and 58 ± 4 kJ/mol. These values can be converted to 0 K bond energies for comparison to our threshold measurements using molecular constants calculated by ab initio theory [54]. These values, 1.11 and 0.57 ± 0.04 eV, respectively, are also shown in Figure 7 by the arrows. Clearly, the HPMS values agree nicely with the onsets of the unconvoluted models (dashed lines), but not with the apparent thresholds. Average internal energies of these two clusters at room temperature are 0.11 and 0.38 eV, respectively, values that account for much of the difference between the unconvoluted and convoluted models. Without including vibrational energy in the analysis

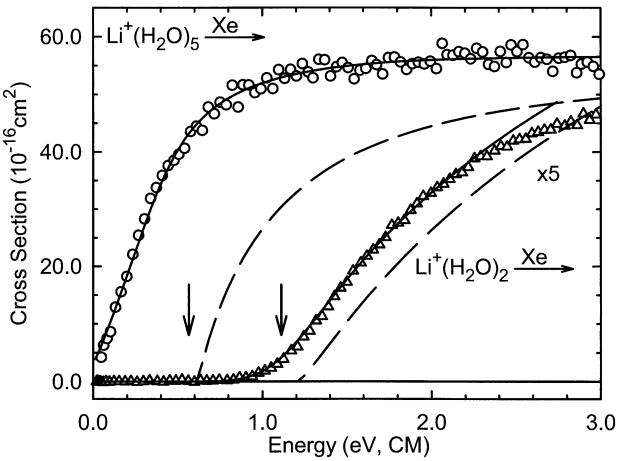

Figure 7. Experimental cross sections for collision-induced dissociation of $Li^+(H_2O)_2$ (expanded by a factor of five) and $Li^+(H_2O)_5$ with Xe as a function of center-of-mass energy. The dashed lines show the model of eq 9 for reactants with no internal energy. The full lines show these models including the internal energy distributions and convoluted with the kinetic energy distributions of the reactants. Arrows indicate the bond energies for these complexes measured by equilibrium methods at 1.11 and 0.57 eV, respectively [54].

of these data, bond energies for the $Li^+(H_2O)_x$ complexes would differ appreciably from those determined by equilibrium methods. When these internal energies are included, bond energies obtained by CID and HPMS agree within experimental uncertainty for $x = 2$, 3, 4, and 5 (no value was measured by HPMS for $x = 1$). These values also agree well with high level ab initio calculations [54]. Similar agreement has been obtained for a variety of other complexes, making it clear that vibrational and translational energy are both available to drive reactions.

Internal Energy of the Reactants: Rotational

Elucidating the influence of rotational energy on reaction thermochemistry is even more difficult than for vibrational energy because the amounts are so small. Contributions can be $k_BT/2$ (0.013 eV at 298 K) for each rotational degree of freedom in the reactants, leading to a maximum total rotational energy contribution of 0.08 eV for two nonlinear reactants. Conceptually, including rotational energy seems reasonable as the collision event can thoroughly mix the various sources of energy available to the reactants. Conservation of angular momentum could conceivably limit how much rotational energy is available, but rotational angular momentum is mixed with the orbital angular momenta of the reactants and products, and the latter are ordinarily much larger. In most systems studied experimentally, the rotational energies are comparable or less than the uncertainties in any threshold determinations, such that comparisons with other experiments or theory cannot provide a definitive answer. In a few cases, it has been demonstrated that rotational energy is available, e.g., in

the reactions of $C^+ + H_2$, HD, D_2 and $N^+ + H_2$, HD, D_2 [18, 55–57]. Viggiano and Morris have concluded that rotational and translational energy are equally available for driving slightly endothermic charge transfer processes [58]. In other cases, the precision afforded by analysis of competitive CID processes (see below) has permitted evaluations which suggest that rotational energy is not active in promoting proton transfer reactions [59, 60]. At present, there are no guiding principles that elucidate which systems should or should not include rotational energy. As there is no good conceptual reason to exclude this source of energy at present, we have consistently included it in our threshold determinations.

To include all sources of reactant internal energy (electronic, vibrational, and rotational), we presently use eq 10 as our standard model.

$$\sigma(E) = \sigma_0 \Sigma g_i (E + E_i - E_0)^n / E \quad (10)$$

Here, there is an explicit sum over all states i representing all rovibrational and electronic states of the reactants with energies E_i and populations g_i, where $\Sigma g_i = 1$. This requires molecular parameters (electronic, vibrational, and rotational constants) of both reactants along with information regarding the populations of these states. These parameters can be experimental values when available or obtained from ab initio calculations. To properly define the populations, we note that the neutral is usually at room temperature and when the flow tube source is used to generate ions, the ions can also be characterized as having a room temperature internal energy distribution. A well-characterized ion source is therefore a key component in accurate thermodynamic work.

Single versus Multiple Collisions

In many circumstances, the pressure in the collision cell can be operated low enough that the probability of secondary collisions is sufficiently small so that resulting perturbations in the reaction cross sections are small. However, *experimentally, there is no such thing as truly single collision conditions.* Unless there is only a single neutral reactant molecule in the collision cell, there is always a finite probability that a reactant ion can undergo sequential collisions with the reactant neutrals. Even though true single collision conditions cannot be achieved in the laboratory, reaction cross sections for single collisions can be measured straightforwardly by extrapolating cross sections measured at different pressures to the zero pressure limit, rigorously single collision conditions.

Does it matter whether multiple collisions take place? If you are trying to obtain accurate threshold information, then the answer is a definitive yes, unless you explicitly account for multiple collisions in the modeling. The advantage of dealing with single collisions is that the energy of the ion-molecule reaction is well defined, whereas in multiple collisions, each collision leads to increased variability in the distribution of reactant velocities. The effects of multiple collisions can be most obvious in bimolecular reactions, as was apparent in some of our earliest studies [6, 21, 55]. For example, in the reaction of $Ar^+ + H_2$, the dominant product channel is $ArH^+ + H$, but charge transfer is also observed at low energies [6]. The H_2^+ product of this reaction goes on to react with H_2 to form $H_3^+ + H$ very efficiently. Clearly, H_3^+ cannot be formed in a single bimolecular encounter between Ar^+ and H_2. Examination of the pressure dependence of these processes shows that the intensities of the ArH^+ and H_2^+ product ions increases linearly with pressure, as expected for eq 6 at low pressures. In contrast, the H_3^+ intensity increases quadratically, as expected for the product of a secondary reaction. The slope of these lines at zero pressure accurately gives the single collision cross sections. Alternatively, one can convert the intensities to apparent cross sections using eq 6. Then, $\sigma(ArH^+)$ and $\sigma(H_2^+)$ are found to be constants at low H_2 pressures, whereas $\sigma(H_3^+)$ increases linearly with pressure and is zero at zero pressure. Hence, an extrapolation of the cross sections to zero pressure provides the required single collision cross sections.

A somewhat more subtle pressure effect is observed for CID reactions because here the product ions do not change. However, multiple collisions can deposit more energy than a single collision at the same laboratory ion energy such that the threshold for product formation in reaction 2 shifts to lower energies. This effect is systematic and omnipresent, although some systems are more sensitive than others, for reasons outlined below. An example of this pressure effect is shown in Figure 8 for the CID of Na^+(benzene) with Xe. Results for two pressures of Xe (0.07 and 0.20 mTorr) are shown and correspond to single collision probabilities in our instrument of 2.5 and 8%, respectively (calculated using eq 6 with the cross section measured at high energies, 15 $Å^2$). Extrapolating these results (along with results for an intermediate pressure, not shown for clarity) to zero pressure of Xe yields the line shown in Figure 8. Analyses of these three data sets finds thresholds that are shifted to lower energies by 0.04 eV at 0.07 mTorr and 0.10 eV at 0.20 mTorr. Thus, even though the results shown correspond to what is generally considered single collision conditions, i.e., the probabilities of secondary collisions are only 0.6% at the highest pressure, the effects of secondary collisions definitely skew the measured thresholds. Further, Figure 8 illustrates that the observation of such pressure effects is subtle and requires high precision data, but the effects on the threshold analysis are distinct. Ultimately, analysis of CID data that has not been corrected in this fashion provides only a lower limit to the correct thermochemistry.

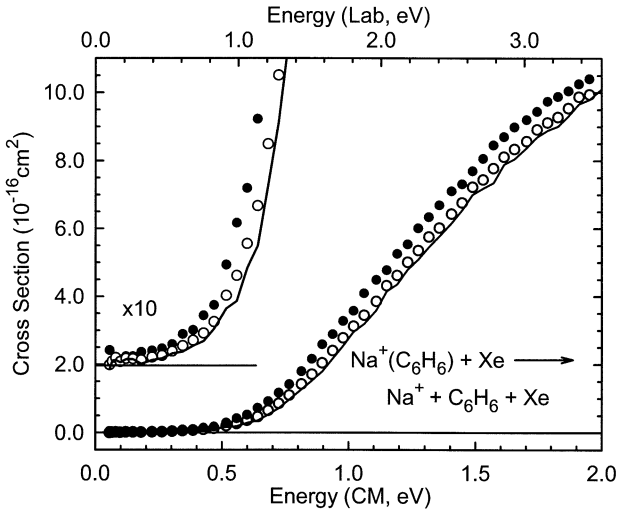

Figure 8. Experimental cross sections for collision-induced dissociation of $Na^+(C_6H_6)$ with Xe as a function of laboratory ion energy, upper x-axis, and center-of-mass energy, lower x-axis. Data obtained at a pressure of 0.07 (open circles) and 0.20 (closed circles) mTorr of Xe are shown. The line is an extrapolation of these data to zero pressure of Xe, rigorously single collision conditions.

Collision Partner in Collision-Induced Dissociation

The neutral reagent in collision-induced dissociation experiments, Rg in reaction 2, is optimally chosen to provide efficient kinetic to internal energy transfer during the collision, while minimizing the amount of energy removed after the collision. Both principles can be realized if there are long-lived collisions in which the transient $M^+(A)(Rg)$ complex dissociates statistically. Presuming the ligand A is modestly complex, there are many more internal modes than translational modes such that statistical behavior puts most of the reactant kinetic energy into internal energy of the complex. (This has been explicitly demonstrated by kinetic energy release distributions, which find that the maximum kinetic energy of receding products is near zero for statistical dissociations; see for example [61]). The amount of energy removed by Rg can be further reduced by the use of monatomic gases, e.g., the rare gases, which have no internal modes.

In order to maximize the probability that the MA^+ + Rg collision will form a long-lived complex, Rg should bind as strongly as possible to ions. Thus, Rg should be polarizable, and among the rare gases readily available, Xe has the highest polarizability. Therefore, the use of Xe as an efficient collision gas for CID experiments can be rationalized. The relative efficiency of collisional energy transfer with Xe versus the other rare gases has been empirically demonstrated in a number of studies in our group [16, 51, 62–64]. In some cases, we have documented that other competing reactions, e.g., charge transfer [16] or ligand exchange [65, 66], can adversely affect the desired CID process, in which case, one of the lighter rare gases may prove to be a better choice as a collision gas.

Kinetic Shifts

All energized complexes have finite lifetimes for dissociating. Such complexes can be formed in a bimolecular reaction, e.g., reaction 1 forms MAB^+ as a transient intermediate that always has enough energy to dissociate to reactants and, depending on the energetics, may also dissociate to products. Alternatively, collisional energy transfer to MA^+ in the CID reaction 2 can yield MA^+ as the energized complex. In our GIBMS experiments, such energized complexes move through the laboratory towards the detector (otherwise they are never detected) with a time scale of about 10^{-4} s (5×10^{-4} s in the double octopole apparatus). For small molecules, the rates of reaction (dissociation) are sufficiently rapid that MAB^+ is never observed (under single collision conditions) and CID of MA^+ occurs faster than the flight time of the ions once the internal energy of the complex exceeds the bond energy. As the molecules get larger, there are an increased number of places in the complex where energy can be stored that do not lead to reaction. Consequently, the lifetime of the complex increases, and can eventually exceed the experimental timescale. Under these circumstances and for a given sensitivity, the onset for product formation is shifted to higher kinetic energies, resulting in a kinetic shift. Increasing the energy in such long-lived complexes increases the dissociation rate, enhancing the probability of seeing products. Indeed, this effect is why CID processes are particularly sensitive to multiple collisions, because the extra collision deposits additional energy into the complex, such that its dissociation rate can be increased by orders of magnitude at energies near threshold.

If accurate thermochemistry is to be obtained from the analysis of data plagued by kinetic shifts, then the kinetics of dissociation must be included in the analysis. This first became obvious to us in our studies of the CID of transition metal cluster cations [8]. Subsequently, we have refined our treatment upon several occasions [67, 68]. Presently, we use eq 11, which incorporates integration over a unimolecular dissociation probability.

$$\sigma(E) = (n\sigma_0/E) \sum_i g_i \int_0^{E+E_i-E_0} [1 - e^{-k(E+E_i-\Delta E)\tau}] \times (\Delta E)^{n-1}\, d(\Delta E), \quad (11)$$

Here, ΔE is the energy that remains in translation after collision, τ is the average experimental time available for dissociation (the ion time-of-flight from the collision cell to the quadrupole mass analyzer, on average 100 and 500 μs in our two GIBMS instruments), and $k(E + E_i - \Delta E) = k(E^*)$ is the unimolecular dissociation rate constant, calculated using Rice-Ramsperger-Kassel-Marcus (RRKM) statistical theory; see for example [69]. When the dissociation rate, $k(E^*)$, is faster than the

time-of-flight of the ions, as for smaller ions, this integration recovers eq 10.

Information necessary to utilize this model are molecular parameters for the energized molecules (for CID reactions, this is the same information needed to assess the internal energies of the reactant ions) and for the transition state (TS) leading to products. For many processes, we have argued [68] that the latter can be accurately assessed assuming that the TS is loose and located at the centrifugal barrier for product formation, a so-called orbiting TS or phase space limit TS. This should be true as long as the threshold for dissociation corresponds to the asymptotic products, which is generally true for ion-molecule systems for the reasons discussed above. In cases where a tight TS and barriers are involved, this may be identified and the molecular parameters provided by ab initio calculations. In such circumstances, the threshold obtained corresponds to the energy of the transition state, and no longer to the product asymptote.

Our metal cluster cation work provided the first examples of systems where the influence of kinetic shifts was obvious [8, 70, 71]. In these cases, thresholds for dissociation of M_x^+ clusters would increase gradually until they exceeded bulk phase heats of vaporization by factors of two for the largest clusters studied. When kinetic shifts were included in our analysis, the M_x^+ bond energies would approach the bulk phase limit for these larger clusters. Our best test of the accuracy of these values is to examine the cohesive energies of the clusters, defined as the sum of the bond energies divided by the number of atoms. When kinetic shifts are included, these values extrapolate to the bulk phase heat of vaporization within 10% [71].

Another striking example of the need to assess kinetic shifts is shown in Figure 9 for dissociation of the complex of Na^+ with the 18–crown–6 cyclic polyether [72, 73]. Here the apparent threshold is about 6 eV, whereas analysis performed using eq 10 (without kinetic shifts) gives a threshold of 7.37 ± 0.24 eV. Using eq 11 (with kinetic shifts) yields a threshold of 3.07 ± 0.20 eV, which can be favorably compared with results from ab initio theory of 3.44 eV [74]. (Indeed, at the level of theory used, the bond energies of Na^+ to other simple ethers, where kinetic shifts should not be influential, are systematically overestimated by 12 ± 8%, which corresponds to a shift of 0.37 ± 0.25 eV in the 18–crown–6 system [73].) Such systems make it evident that kinetic shifts must be included in the analysis of such larger complexes. However, it should be realized that the accuracy of the estimated kinetic shift is limited by the models used, including statistical RRKM theory, and the assumptions made regarding the transition states for the appropriate dissociation. In our work, generous uncertainties are assigned to the molecular parameters used in evaluating the kinetic shifts, which should provide reasonable uncertainties in the final threshold values.

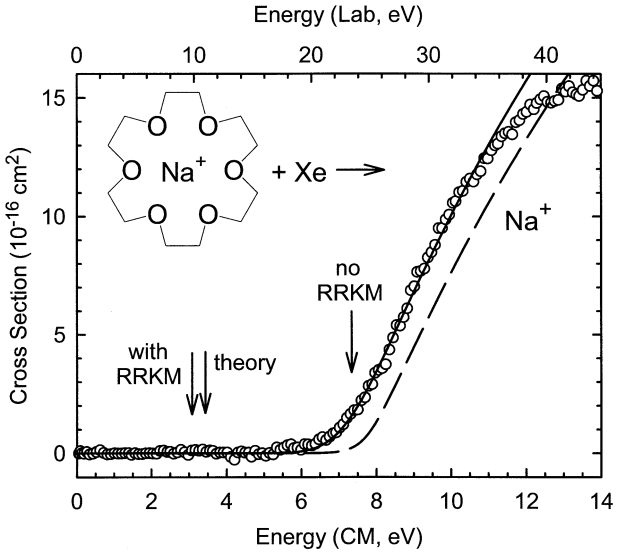

Figure 9. Experimental cross sections for collision-induced dissociation of Na^+(18–crown–6) with Xe as a function of laboratory ion energy, upper x-axis, and center-of-mass energy, lower x-axis. The dashed line shows the model of eq 11 that includes lifetime effects but no internal energies. The full line shows this model convoluted with the kinetic and internal energy distributions of the reactants. Arrows indicate the bond energies for this complex measured using eq 10 (no RRKM, which excludes lifetime effects), using eq 11 (with RRKM), and calculated (theory) [74].

Competitive Shifts

Anytime two or more reactions occur in parallel, there is the possibility that they can compete with one another. Evidence for competition is abundant and may or may not influence the thresholds for reaction. For example, Figure 10 shows results for the reaction of W^+ with perdeuterated methane [75]. The dominant process observed is dehydrogenation, reaction 12, but at higher energies, two additional processes of conse-

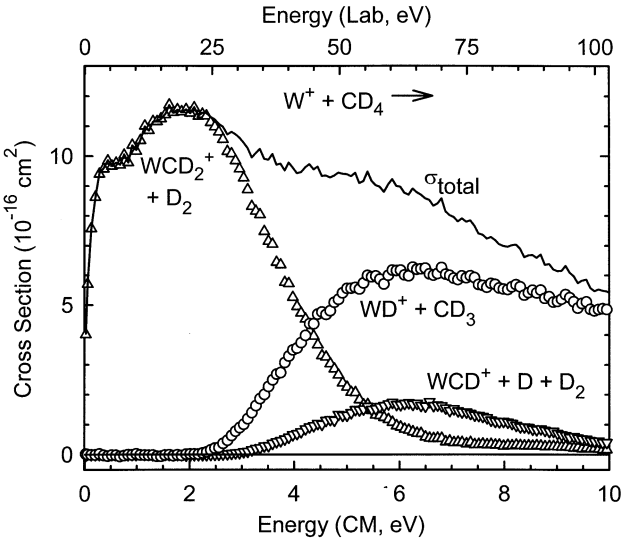

Figure 10. Experimental cross sections for reactions 12–14 (symbols) and their sum (line) as a function of laboratory ion energy, upper x-axis, and center-of-mass energy, lower x-axis.

quence are observed, reactions 13 and 14. (Others are also present but have much smaller cross sections.)

$$W^+ + CD_4 \rightarrow WCD_2^+ + D_2 \quad (12)$$

$$\rightarrow WD^+ + CD_3 \quad (13)$$

$$\rightarrow WCD^+ + D + D_2 \quad (14)$$

It can be seen that the total cross section behaves smoothly with energy, indicating that the sharp decline in the cross section for WCD_2^+ is a result of competition with the other two channels. For reaction 14, this can simply be decomposition of the WCD_2^+ product by loss of a D atom, but $WD^+ + CD_3$ cannot be formed by decomposition of WCD_2^+. The explanation is that all of these reactions occur via the transient intermediate, $D–W^+–CD_3$, which at low energies can rearrange to eliminate D_2 in reaction 12, but at higher energies, can simply break the W–C bond to yield reaction 13. The latter process is kinetically favored such that when its threshold is reached, the intermediate preferentially decomposes along this pathway, thereby reducing the amount of this species that can rearrange to yield reaction 12.

Another example of competition that illustrates the effects on thermochemistry directly is competitive CID, processes 15.

$$(L_1)M^+(L_2) + Rg \rightarrow M^+(L_1) + L_2 + Rg \quad (15a)$$

$$\rightarrow M^+(L_2) + L_1 + Rg \quad (15b)$$

We first studied such processes in bisligated Li^+ complexes of alcohols and water [76]. An example is shown in Figure 11. Here the bond energy of $Li^+(H_2O)$ is only 0.20 ± 0.03 eV weaker than that of $Li^+(CH_3OH)$, yet the appearance of the two cross sections differs appreciably. The lower energy channel, $Li^+(CH_3OH) + H_2O$, has a cross section that rises rapidly and then levels out once the second channel starts. This latter cross section rises much more slowly but continues to rise as energy is increased. The explanation for both behaviors is that the same energized molecule, collisionally excited $(H_2O)Li^+(CH_3OH)$, decomposes into both products. At lower energies, only one pathway is open, $Li^+(CH_3OH) + H_2O$, so this cross section rises rapidly from its thermodynamic threshold. As the threshold for formation of $Li^+(H_2O) + CH_3OH$ is exceeded, the complex can now decompose by two pathways. Statistically, the number of states available to the lower energy channel is much greater than to the higher energy channel, such that the cross section for the second channel rises slowly from its thermodynamic threshold, a victim of competition with the lower energy channel. As this second channel opens, the formation of the first product channel slows, such that the cross section levels out. As the energy increases further, the statistical difference in the two channels diminishes and the magnitudes of the two cross sections approach one another more closely.

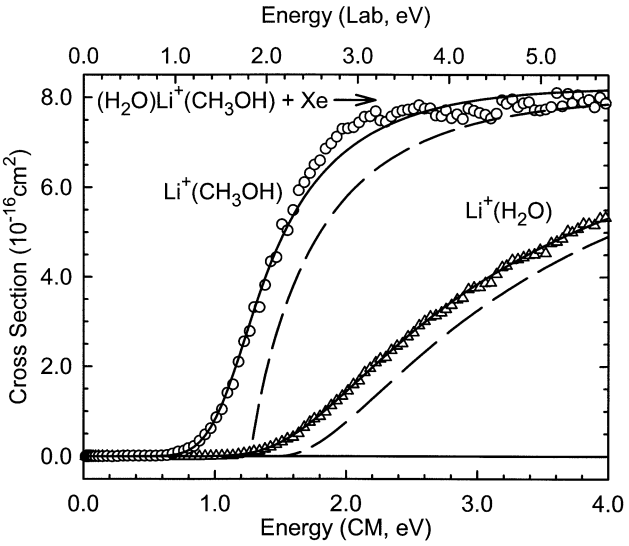

Figure 11. Experimental cross sections for collision-induced dissociation of $(H_2O)Li^+(CH_3OH)$ with Xe as a function of laboratory ion energy, upper x-axis, and center-of-mass energy, lower x-axis. The dashed lines show the model of eq 16 that includes lifetime and competitive effects for reactants with no internal energy. The full lines show these models convoluted with the kinetic and internal energy distributions of the reactants.

To quantify the effect that such competition can have on the threshold determinations of such processes, we have devised a statistical model for simultaneous analysis of such cross sections [76]. This is accomplished using eq 11 as a template and simply including the fact that there are multiple channels available. The equation used to model competitive CID data is

$$\sigma_j(E) = \frac{n\sigma_{0,j}}{E} \sum_i g_i \int_0^{E+E_i-E_0} \frac{k_j(E^*)}{k_{tot}(E^*)}[1 - e^{-k_{tot}(E^*)\tau}] \times (\Delta E)^{n-1}\, d(\Delta E), \quad (16)$$

where indices j refer to a particular product channel and $k_{tot} = \Sigma k_j$, where all rate constants are calculated using RRKM theory. The ratio of dissociation rates k_j/k_{tot} introduces the coupling between product channels j. The scaling factors $\sigma_{0,j}$ are ideally the same for all product channels. Our early work [76] indicated that separate scaling was sometimes needed in order to model the data well, however, more recent work identifies additional statistical factors (e.g., the symmetry numbers of internal rotors) that are needed to provide accurate modeling of the competition without the need for empirical scaling factors [77].

In the case shown in Figure 11, independent analyses of these two product cross sections yield a difference in thresholds of 0.47 ± 0.07 eV, whereas simultaneous analysis of both channels using eq 16 provides a difference of 0.24 ± 0.01 eV. This value agrees well with our

recommended difference of 0.20 ± 0.03 eV, which is obtained by combining the relative threshold information along with directly measured bond energies for $Li^+(H_2O)$ and $Li^+(CH_3OH)$, which differ by 0.23 ± 0.16 eV [78], and relative values from equilibrium measurements, 0.20 eV [79]. Note that the precision of such a competitive analysis is quite high, a consequence of the requirement that two cross sections must be reproduced simultaneously.

Conclusions

Guided ion beam tandem mass spectrometry has proved to be a versatile means to examine the kinetic energy dependence of a wide variety of ion-molecule reactions. For endothermic processes, an analysis of this dependence can provide thermodynamic information. To ensure that such information is accurate, a number of effects must be carefully considered in the conversion of the raw data to instrument-independent cross sections and then in elucidating the thresholds for reaction. These effects are illustrated and outlined in this manuscript. The resulting thermodynamic information has been verified in many systems throughout the years, both by comparison to other experiments and to theory. In many cases, however, such thermochemistry is unavailable from other sources, and it is here that reliable GIBMS studies can have the strongest impact.

However, lists of thermodynamic information are only the beginning. By providing comprehensive thermochemistry on many related systems, insight into the multitude of factors that control and influence bond energies can be provided. Elucidating such trends allows substantial predictive capabilities that transcend the gas-phase environment where the thermochemistry is measured. It is this descriptive information that provides part of the intellectual challenge and the driving force for much of our work. Unfortunately, a review of the many stories that lie behind the thermochemistry is beyond the scope of this article. Such thermodynamic information has been compiled, reviewed, and coupled with explanations of the trends in a number of recent sources. These include a reassessment of all our early transition metal work [80], an updated version that focuses on transition metal carbon bond energies [81], articles that involve only transition metal clusters [71, 82], a review of our transition metal sulfide thermochemistry [83], and a recent comprehensive review of noncovalent metal–ligand bond energies 84].

Acknowledgments

The author thanks the National Science Foundation and the Department of Energy, Office of Basic Energy Sciences for continued support in the areas discussed in this work. He would particularly like to acknowledge the hard work, dedication, and insight of a great group of students, postdocs, and collaborators. Many of them are included in the references herein and it is indeed an honor to have several of them join him as authors in this issue.

References

1. Lias, S. G.; Bartmess, J. E. In *Gas-Phase Ion Thermochemistry. NIST Chemistry WebBook, NIST Standard Reference Database Number 69*; Mallard, W. G.; Linstrom, P. J. Eds.; National Institute of Standards and Technology: Gaithersburg, 2000; (http://webbook.nist.gov).
2. Talrose, V. L.; Vinogradov, P. S.; Larin, I. K. On the Rapidity of Ion-molecule Reactions. Bowers, M. T., Ed. *In Gas Phase Ion Chemistry, Vol. I.* Academic: New York, 1979; p 305–347.
3. Armentrout, P. B. Thermochemical Measurements by Guided Ion Beam Mass Spectrometry. Adams, N. G.; Babcock, L. M., Eds. *In Advances in Gas Phase Ion Chemistry, Vol. I.* JAI: Greenwich, 1992; pp 83–119.
4. Armentrout, P. B.; Halle, L. F.; Beauchamp, J. L. Reactions of Cr^+, Mn^+, Fe^+, Co^+, and Ni^+ with O_2 and N_2O. Examination of the Translational Energy Dependence of the Cross Sections of Endothermic Reactions. *J. Chem. Phys.* **1982,** *76,* 2449–2457.
5. Armentrout, P. B.; Simons, J. Understanding Heterolytic Bond Cleavage. *J. Am. Chem. Soc.* **1992,** *114,* 8627–8633.
6. Ervin, K. M.; Armentrout, P. B. Translational Energy Dependence of $Ar^+ + XY \rightarrow ArX^+ + Y$ (XY = H_2, D_2, HD) from Thermal to 30 eV cm. *J. Chem. Phys.* **1985,** *83,* 166–189.
7. Muntean, F.; Armentrout, P. B. Guided Ion Beam Study of Collision-Induced Dissociation Dynamics: Integral and Differential Cross Sections. *J. Chem. Phys.* **2001,** *115,* 1213–1228.
8. Loh, S. K.; Hales, D. A.; Lian, L.; Armentrout, P. B. Collision-Induced Dissociation of Fe_n^+ ($n = 2 - 10$) with Xe: Ionic and Neutral Iron Cluster Binding Energies. *J. Chem. Phys.* **1989,** *90,* 5466–5485.
9. Hansen, S. G.; Farrar, J. M.; Mahan, B. H. Dynamics of the Reaction of N^+ with H_2. V. Reactive and Nonreactive Scattering of $N^+(^3P)$ at Relative Energies Below 3.6 eV. *J. Chem. Phys.* **1980,** *73,* 3750–3762.
10. Gerlichm D. Diplomarbeit, University of Freiburg, Federal Republic of Germany, 1971, p 1.
11. Teloy, E.; Gerlich, D. Integral Cross Sections for Ion-molecule Reactions. I. The Guided Beam Technique. *Chem. Phys.* **1974,** *4,* 417–427.
12. Gerlich, D. Inhomogeneous rf Fields: A Versatile Tool for the Study of Processes with Slow Ions. In *State-Selected and State-to-State Ion-Molecule Reaction Dynamics. Part I, Experiment*; Ng, C.-Y.; Baer, M., Eds.; 1992; pp 1–176.
13. Chiu, Y.; Fu, H.; Huang, J.; Anderson, S. L. Vibrational Mode Effects, Scattering Dynamics, and Energy Disposal in Reaction of $C_2H_2^+$ with Methane. *J. Chem. Phys.* **1995,** *102,* 1199–1216.
14. Williams, S.; Chiu, Y.-H.; Levandier, D. J.; Dressler, R. A. Determination of Photofragment Ion Translational Energy and Angular Distributions in an Octopole Ion Guide: A Case Study of the Ar_2^+ and $(N_2O^{\cdot}H_2O)^+$ Cluster Ions. *J. Chem. Phys.* **1998,** *109,* 7450–7461.
15. Daly, N. R. Scintillation Type Mass Spectrometer Ion Detector. *Rev. Sci. Instrum.* **1960,** *31,* 264–267.
16. Schultz, R. H.; Armentrout, P. B. Reactions of N_4^+ with Rare Gases from Thermal to 10 eV Center-of-Mass Energy: Collision-Induced Dissociation, Charge Transfer, and Ligand Exchange. *Int. J. Mass Spectrom. Ion Processes* **1991,** *107,* 29–48.
17. Loh, S. K.; Hales, D. A.; Armentrout, P. B. A Continuous Source for Production of Cold, Mass-Selected Transition Metal Cluster Ions. *Chem. Phys. Lett.* **1986,** *129,* 527–532.
18. Ervin, K. M.; Armentrout, P. B. Threshold Behavior of Endothermic Reactions: $C^+(^2P) + H_2 \rightarrow CH^+ + H$. *J. Chem. Phys.* **1984,** *80,* 2978–2980.
19. Huber, K. P.; Herzberg, G. *Molecular Spectra and Molecular Structure. IV. Constants of Diatomic Molecules.* Van Nostrand Reinhold: New York, 1979, pp 240, 262.
20. Zhang, X.-G.; Rue, C.; Shin, S.-Y.; Armentrout, P. B. Reactions of Ta^+ and W^+ with H_2, D_2, and HD: Effect of Lanthanide

Contraction and Spin-Orbit Interactions on Reactivity and Thermochemistry. *J. Chem. Phys.* Submitted for publication.
21. Burley, J. D.; Ervin, K. M.; Armentrout, P. B. Translational Energy Dependence of $O^+(^4S) + H_2(D_2, HD) \rightarrow OH^+(OD^+) + H(D)$ from Thermal to 30 eV c.m. *Int. J. Mass Spectrom. Ion Processes* **1987,** *80,* 153–175.
22. Schultz, R. H.; Armentrout, P. B. Hydrogen Atom Transfer Reactions of N_2^+ with H_2, HD, and D_2 from Thermal to 10 eV cm. *J. Chem. Phys.* **1992,** *96,* 1036–1045.
23. Turner, B. R.; Fineman, M. A.; Stebbings, R. F. Crossed-Beam Investigation of N_2D^+ Production in N_2^+-D_2 Collisions. *J. Chem. Phys.* **1965,** *42,* 4088–4096.
24. Hierl, P. M.; Strattan, L. W.; Wyatt, J. R. A Chemical Accelerator for the Study for the Dynamics of Ion-Molecule Reactions Over the Energy Range 0.1–100 eV. *Int. J. Mass Spectrom. Ion Phys.* **1972/3,** *10,* 385–403.
25. Gioumousis, G.; Stevenson, D. P. Reactions of Gaseous Molecule Ions with Gaseous Molecules. V. Theory. *J. Chem. Phys.* **1958,** *29,* 294–299.
26. Armentrout, P. B. The Kinetic Energy Dependence of Ion-Molecule Reactions: Guided Ion Beams and Threshold Measurements. *Int. J. Mass Spectrom.* **2000,** *200,* 219–241.
27. Chesnavich, W. J.; Bowers, M. T. Theory of Translationally Driven Reactions. *J. Phys. Chem.* **1979,** *83,* 900.
28. Stowe, G. F.; Schultz, R. H.; Wight, C. A.; Armentrout, P. B. Translational and Electronic Energy Dependence of $S^+ + H_2(D_2, HD) \rightarrow SH^+(SD^+) + H(D)$. Spin-Allowed and Spin-Forbidden Pathways. *Int. J. Mass Spectrom. Ion Processes* **1990,** *100,* 177–195.
29. Rue, C.; Armentrout, P. B.; Kretzschmar, I.; Schröder, D.; Harvey, J. N.; Schwarz, H. Kinetic-Energy Dependence of Competitive Spin-Allowed and Spin-Forbidden Reactions: $V^+ + CS_2$. *J. Chem. Phys.* **1999,** *110,* 7858–7870.
30. Dressler, R. A.; Arnold, S. T.; Murad, E. Charge-Transfer Dynamics in Ion–Polyatomic Molecule Collisions: $X^+ + H_2O$ (X = N, Kr) Luminescence Study. *J. Chem. Phys.* **1995,** *103,* 9989–10000.
31. (a)Landau, L. D. Non-Adiabatic Crossing of Energy Levels. *Phys. Z. Sowjetunion* **1932,** *2,* 46.(b)Zener, C. *Proc. R. Soc. London Ser. A* **1932,** *137,* 696–702.
32. Baer, T.; Hase, W. L. *Unimolecular Reaction Dynamics.* Oxford: New York, 1996; p 316 and references therein.
33. Heller, E. J.; Brown, R. C. Radiationless Transitions in a New Light. *J. Chem. Phys.* **1983,** *79,* 3336–3351.
34. Lorquet, J. C.; Leyh-Nihant, B. Nonadiabatic Unimolecular Reactions. 1. A Statistical Formulation for the Rate Constants. *J. Phys. Chem.* **1988,** *92,* 4778–4783.
35. Chantry, P. J. Doppler Broadening in Beam Experiments. *J. Chem. Phys.* **1971,** *55,* 2746–2759.
36. Lifshitz, C.; Wu, R. L. C.; Tiernan, T. O.; Terwilliger, D. T. Negative Ion-Molecule Reactions of Ozone and Their Implications on the Thermochemistry of O_3^-. *J. Chem. Phys.* **1978,** *68,* 247–260.
37. Ohanessian, G.; Brusich, M. J.; Goddard, W. A., III. Theoretical Study of Transition-Metal Hydrides. V. HfH^+ Through HgH^+, BaH^+, and LaH^+. *J. Am. Chem. Soc.* **1990,** *112,* 7179–7189.
38. Weber, M. E.; Elkind, J. L.; Armentrout, P. B. Kinetic Energy Dependence of $Al^+ + O_2 \rightarrow AlO^+ + O$. *J. Chem. Phys.* **1986,** *84,* 1521–1529.
39. Halle, L. F.; Armentrout, P. B.; Beauchamp, J. L. Formation of Chromium Carbene Ions by Reaction of Electronically Excited Chromium Ions with Methane in the Gas Phase. *J. Am. Chem. Soc.* **1981,** *103,* 962–963.
40. Elkind, J. L.; Armentrout, P. B. Effect of Kinetic and Electronic Energy on the Reaction of V^+ with H_2, HD and D_2. *J. Phys. Chem.* **1985,** *89,* 5626–5636.
41. Elkind, J. L.; Armentrout, P. B. Effect of Kinetic and Electronic Energy on the Reactions of Mn^+ with H_2, HD, and D_2. *J. Chem. Phys.* **1986,** *84,* 4862–4871.
42. Elkind, J. L.; Armentrout, P. B. Effect of Kinetic and Electronic Energy on the Reactions of Fe^+ with H_2, HD, and D_2: State-Specific Cross Sections for $Fe^+(^6D)$ and $Fe^+(^4F)$. *J. Phys. Chem.* **1986,** *90,* 5736–5745.
43. Elkind, J. L.; Armentrout, P. B. Effect of Kinetic and Electronic Energy on the Reactions of Co^+, Ni^+, and Cu^+ with H_2, HD, and D_2. *J. Phys. Chem.* **1986,** *90,* 6576–6586.
44. Rue, C.; Armentrout, P. B.; Kretzschmar, I.; Schröder, D.; Schwarz, H. Guided Ion Beam Studies of the State-Specific Reactions of Cr^+ and Mn^+ with CS_2 and COS. *Int. J. Mass Spectrom.* **2001,** *210/211,* 283–301.
45. Sugar, J.; Corliss, C. Atomic Energy Levels of the Iron-Period Elements: Potassium Through Nickel . *J. Phys. Chem. Ref. Data* **1985,** *14(Suppl. 2),* 1–664.
46. Freas, R. B.; Ridge, D. P. Characterization of Complexes of Butanes with Transition-Metal Atomic Ions in the Gas Phase. *J. Am. Chem. Soc.* **1980,** *102,* 7129–7131.
47. Reents, W. D.; Strobel, F.; Freas, R. B.; Wronka, J.; Ridge, D. P. Chemical Reactions and Collisional Quenching of the Chromium Atomic Ion in a Metastable Excited State. *J. Phys. Chem.* **1985,** *89,* 5666–5670.
48. Georgiadis, R.; Armentrout, P. B. Kinetic Energy Dependence of the Reactions of Ca^+ and Zn^+ with H_2, D_2, and HD. Effect of Empty versus Full d Orbitals. *J. Phys. Chem.* **1988,** *92,* 7060–7067.
49. Fisher, E. R.; Armentrout, P. B. Activation of Alkanes by Cr^+: Unique Reactivity of Ground State $Cr^+(^6S)$ and Thermochemistry of Neutral and Ionic Chromium–Carbon Bonds. *J. Am. Chem. Soc.* **1992,** *114,* 2039–2049.
50. Anderson, S. L. Multiphoton Ionization State Selection: Vibrational-Mode and Rotational-State Control. *Adv. Chem. Phys.* **1992,** *82,* 177–212.
51. Schultz, R. H.; Crellin, K. C.; Armentrout, P. B. Sequential Bond Energies of $Fe(CO)_x^+$ (x = 1–5): Systematic Effects on Collision-Induced Dissociation Measurements. *J. Am. Chem. Soc.* **1991,** *113,* 8590–8601.
52. Rodgers, M. T.; Armentrout, P. B. Collision-Induced Dissociation Measurements on $Li^+(H_2O)_n$, n = 1–6: The First Direct Measurement of the Li^+–OH_2 Bond Energy. *J. Phys. Chem. A* **1997,** *101,* 1238–1249.
53. Dzidic, I.; Kebarle, P. Hydration of the Alkali Ions in the Gas Phase. Enthalpies and Entropies of Reactions $M^+(H_2O)_{n-1} + H_2O = M^+(H_2O)_n$. *J. Phys. Chem.* **1970,** *74,* 1466–1474.
54. Feller, D.; Glendening, E. D.; Kendall, R. A.; Peterson, K. A. An Extended Basis Set ab Initio Study of $Li^+(H_2O)_n$, n = 1–6. *J. Chem. Phys.* **1994,** *100,* 4981–4997.
55. Ervin, K. M.; Armentrout, P. B. Energy Dependence, Kinetic Isotope Effects, and Thermochemistry of the Nearly Thermoneutral Reactions of $N^+ + H_2 \rightarrow NH^+ + H$. *J. Chem. Phys.* **1987,** *86,* 2659–2673.
56. Sunderlin, L. S.; Armentrout, P. B. Rotational Temperature Dependence of the Reaction of N^+ and C^+ with H_2, HD, and D_2. *J. Chem. Phys.* **1994,** *100,* 5639–5645.
57. Tosi, P.; Dimitriev, O.; Bassi, D.; Wick, O.; Gerlich, D. Experimental Observation of the Energy Threshold in the Ion-Molecule Reaction $N^+ + D_2 \rightarrow ND^+ + D$. *J. Chem. Phys.* **1994,** *100,* 4300–4307.
58. Viggiano, A. A.; Morris, R. A. Rotational and Vibrational Energy Effects on Ion-Molecule Reactivity as Studied by the VT-SIFDT Technique. *J. Phys. Chem.* **1996,** *100,* 19227–19240.
59. DeTuri, V. F.; Su, M. A.; Ervin, K. M. Dynamics of Endoergic Bimolecular Proton Transfer Reactions. $F^- + ROH \rightarrow HF + RO^-$ [R = H, CH_3, CH_3CH_2, $(CH_3)_2CH$, and $(CH_3)_3C$]. *J. Phys. Chem. A.* **1999,** *103,* 1468–1479.

60. DeTuri, V. F.; Ervin, K. M. Energetics of Endoergic Proton Transfer Reactions of Anions. *J. Phys. Chem. A.* Submitted for publication.
61. van Koppen, P. A. M.; Bowers, M. T.; Beauchamp, J. L.; Dearden, D. V. Organometallic Reaction Energetics from Product Kinetic Energy Release Distributions. *ACS Symposium Series* **1990,** *428,* 34–54.
62. Aristov, N.; Armentrout, P. B. Collision Induced Dissociation of Vanadium Monoxide Ion. *J. Phys. Chem.* **1986,** *90,* 5135–5140.
63. Hales, D. A.; Armentrout, P. B. Effect of Internal Excitation on the Collision-Induced Dissociation and Reactivity of Co_2^+. *J. Cluster Science* **1990,** *1,* 127–142.
64. Dalleska, N. F.; Honma, K.; Sunderlin, L. S.; Armentrout, P. B. Solvation of Transition Metal Ions by Water. Sequential Binding Energies of $M^+(H_2O)_x$ (x = 1–4) for M = Ti–Cu Determined by Collision-Induced Dissociation. *J. Am. Chem. Soc.* **1994,** *116,* 3519–3528.
65. Andersen, A.; Muntean, F.; Walter, D.; Rue, C.; Armentrout, P. B. Collision-Induced Dissociation and Theoretical Studies of Mg^+ Complexes with CO, CO_2, NH_3, CH_4, CH_3OH, and C_6H_6. *J. Phys. Chem. A* **2000,** *104,* 692–705.
66. Tjelta, B. L.; Walter, D.; Armentrout, P. B. Determination of Weak Fe^+–L Bond Energies (L = Ar, Kr, Xe, N_2, CO_2) by Ligand Exchange Reactions and Collision-Induced Dissociation. *Int. J. Mass Spectrom.* **2001,** *204,* 7–21.
67. Khan, F. A.; Clemmer, D. E.; Schultz, R. H.; Armentrout, P. B. The Sequential Bond Energies of $Cr(CO)_x^+$, x = 1–6. *J. Phys. Chem.* **1993,** *97,* 7978–7987.
68. Rodgers, M. T.; Ervin, K. M.; Armentrout, P. B. Statistical Modeling of Collision-Induced Dissociation Thresholds. *J. Chem. Phys.* **1997,** *106,* 4499–4508.
69. Gilbert, R. G.; Smith, S. C. *Theory of Unimolecular and Recombination Reactions.* Blackwell Scientific Publications: Oxford, 1990, p 1.
70. Lian, L.; Su, C.-X.; Armentrout, P. B. Collision-Induced Dissociation of Ni_n^+ (n = 2–18) with Xe: Bond Energies, Geometrical Structures, and Dissociation Pathways. *J. Chem. Phys.* **1992,** *96,* 7542–7554.
71. Armentrout, P. B.; Hales, D. A.; Lian, L. Collision-Induced Dissociation of Transition Metal Cluster Ions. Duncan, M. A., Ed. *In Advances in Metal and Semiconductor Clusters, Vol. II.* JAI: Greenwich, 1994; pp 1–39.
72. More, M. B.; Ray, D.; Armentrout, P. B. Intrinsic Affinities of Alkali Cations for 15–Crown–5 and 18–Crown–6: Bond Dissociation Energies of Gas-Phase M^+–Crown Ether Complexes. *J. Am. Chem. Soc.* **1999,** *121,* 417–423.
73. Armentrout, P. B. Cation-Ether Complexes in the Gas Phase: Thermodynamic Insight into Molecular Recognition. *Int. J. Mass Spectrom.* **1999,** *193,* 227–240.
74. Glendening, E. D.; Feller, D.; Thompson, M. A. An ab Initio Investigation of the Structure and Alkali Metal Cation Selectivity of 18–Crown–6. *J. Am. Chem. Soc.* **1994,** *116,* 10657–10669.
75. Shin, S.-Y.; Armentrout, P. B. Unpublished work.
76. Rodgers, M. T.; Armentrout, P. B. Statistical Modeling of Competitive Threshold Collision-Induced Dissociation. *J. Chem. Phys.* **1998,** *109,* 1787–1800.
77. Amicangelo, J. C.; Armentrout, P. B. Relative and Absolute Bond Dissociation Energies of Sodium Cation Complexes Determined Using Competitive Collision-Induced Dissociation Experiments. *Int. J. Mass Spectrom.* In press.
78. Rodgers, M. T.; Armentrout, P. B. Absolute Binding Energies of Lithium Ions to Short Chain Alcohols. *J. Phys. Chem. A* **1997,** *101,* 2614–2625.
79. Taft, R. W.; Anvia, F.; Gal, J.-F.; Walsh, S.; Capon, M.; Holmes, M. C.; Hosn, K.; Oloumi, G.; Vasanwala, R.; Yazdani, S. Free Energies of Cation-Molecule Complex Formation and of Cation-Solvent Transfers. *Pure Appl. Chem.* **1990,** *62,* 17–23.
80. Armentrout, P. B.; Kickel, B. L. Gas-Phase Thermochemistry of Transition Metal Ligand Systems: Reassessment of Values and Periodic Trends. *In Organometallic Ion Chemistry;* Freiser, B. S., Ed.; Kluwer: Dordrecht, 1996; pp 1–45.
81. Armentrout, P. B. Gas Phase Organometallic Chemistry. Brown, J. M.; Hofmann, P., Eds. *In Organometallic Bonding and Reactivity. Topics in Organometallic Chemistry, Vol. IV.* Springer-Verlag: Berlin, 1999; pp 1–45.
82. Armentrout, P. B. Reactions and Thermochemistry of Small Transition Metal Cluster Ions. *Ann. Rev. Phys. Chem.* **2001,** *52,* 423–461.
83. Rodgers, M. T.; Armentrout, P. B. Noncovalent Metal–Ligand Bond Energies as Studied by Threshold Collision-Induced Dissociation. *Mass Spectrometry Reviews* **2000,** *19,* 215–247.
84. Kretzschmar, I.; Schröder, D.; Schwarz, H.; Armentrout, P. B. The Binding in Neutral and Cationic 3d and 4d Transition-Metal Monoxides and -Sulfides. In *Advances in Metal and Semiconductor Clusters Vol. 5; Duncan, M. A., Ed.; JAI: Greenwich, 2001; pp 347–394.*